applied sciences

MDPI

Article

A Weakly-Coupled Double Bow-Tie Multi-Ring Elliptical Core Multi-Mode Fiber for Mode Division Multiplexing across C+L+U Band

Yingjuan Ci [1], Fang Ren [1,2,*], Xiao Lei [1], Yidan Li [1], Deyang Zhou [1] and Jianping Wang [1,2]

[1] School of Computer and Communication Engineering, University of Science and Technology Beijing, Beijing 110108, China; ciyingjuan@163.com (Y.C.); leixiao1368405503@163.com (X.L.); 13472281135@163.com (Y.L.); zoeyi1213@163.com (D.Z.); jpwang@ustb.edu.cn (J.W.)

[2] Beijing Engineering and Technology Research Center for Convergence Networks and Ubiquitous Services, University of Science and Technology Beijing, Beijing 110108, China

* Correspondence: renfang@ustb.edu.cn

Abstract: We herein present a weakly-coupled double bow-tie multi-ring elliptical core multi-mode fiber (DBT-MREC-MMF) supporting 22 eigenmodes for mode division multiplexing across the C+L+U band. The proposed fiber introduces a multi-ring elliptical core, bow-tie air holes, and bow-tie stress-applying areas to effectively split adjacent eigenmodes. By utilizing the finite element method (FEM), we accordingly optimized the fiber to support the 22 modes under the weakly-coupled condition. We evaluated the impact of fiber parameters on the minimum effective refractive index difference (min Δn_{eff}) between adjacent eigenmodes, model birefringence (B_{m}), and bending loss at a wavelength of 1550 nm. Additionally, broadband performance metrics, such as effective modal index (n_{eff}), effective index difference (Δn_{eff}), effective mode area (A_{eff}), differential mode delay (DMD), and chromatic dispersion (D), were comprehensively studied over the entire C+L+U band, ranging from 1530 to 1675 nm. The proposed fiber is capable of supporting 22 completely separated eigenmodes with a min Δn_{eff} between adjacent eigenmodes larger than 3.089×10^{-4} over the entire C+L+U band. The proposed DBT-MREC-MMF holds great potential for use in short-haul communication systems that require MDM to improve transmission capacity and expand bandwidth.

Keywords: optical fiber; weakly coupled multi-mode fiber; short-haul communication; mode-division multiplexing

Citation: Ci, Y.; Ren, F.; Lei, X.; Li, Y.; Zhou, D.; Wang, J. A Weakly-Coupled Double Bow-Tie Multi-Ring Elliptical Core Multi-Mode Fiber for Mode Division Multiplexing across C+L+U Band. *Appl. Sci.* **2023**, *13*, 5855. https://doi.org/10.3390/app13105855

Academic Editor: Habib Hamam

Received: 14 April 2023
Revised: 8 May 2023
Accepted: 8 May 2023
Published: 9 May 2023

1. Introduction

The exponential growth of new data traffic, social networks, and rapid technological advancements has stimulated the need to expand the capacity of optical fiber communication [1–3]. However, the transmission capacity of traditional single-mode fiber has approached the nonlinear Shannon limit [4,5]. The development of space division multiplexing (SDM) technology has been instrumental in overcoming the limitations of traditional single-mode fiber transmission [6,7]. SDM, using few-mode fiber (FMF) and multi-core fiber (MCF), has been shown to significantly improve transmission system capacity [8,9]. In particular, few-mode fibers (FMFs) in mode division multiplexing (MDM) systems are one of ways to break through the limitations of traditional single mode fiber. However, mode coupling-induced crosstalk remains a key challenge in MDM transmission using FMFs, necessitating a complex and costly multi-input multi-output (MIMO) digital signal processing (DSP) system for effective mitigation [10–12]. To reduce or even eliminate the need for MIMO-DSP, enlarging the mode effective refractive index difference between degenerate modes to larger than 10^{-4} is a promising approach [13].

There have been several works on weakly coupled FMFs, including the ring core fiber [14], elliptical core fiber [15], elliptical ring core fiber [16–18], panda type fiber [19],

bow-tie type fiber [20], and air hole fiber [21–23]. While the previously proposed weakly-coupled FMFs have demonstrated promising characteristics for mode division multiplexing, they still have limitations in terms of the number of supported eigenmodes and bandwidth. For example, Zhang et al. [24] proposed a panda-type separated-circles-formed elliptical ring core FMF capable of supporting 10 modes, with a min Δn_{eff} of 1.2×10^{-4} over the whole C+L band. Du et al. [25] proposed a segmented ring-core panda-type fiber, which also supports 10 modes, with a min Δn_{eff} of 3.5×10^{-4} over the whole C+L band. Yang et al. [26] proposed a bow-tie ring-core FMF that can support 14 modes, with a min Δn_{eff} of 1.6×10^{-4} over the whole C+L band. Behera et al. [27] proposed an M-type few-mode fiber that supports 10 modes, with a min Δn_{eff} of 5×10^{-3} over the C band. Han et al. [28] proposed a cladding rods-assisted depressed-core FMF that supports nine modes, with a min Δn_{eff} of 1×10^{-3} over the C band. However, the number of eigenmodes and bandwidth supported by the fiber need to be further improved.

In this paper, we propose a weakly-coupled double bow-tie multi-ring elliptical core multi-mode fiber supporting 22 eigenmodes across the C+L+U band. The multi-ring elliptical core, bow-tie air holes, and symmetrical bow-tie stress-applying areas improve modal birefringence and effectively separate two adjacent degenerate modes. In particular, the introduction of a multi-ring elliptical fiber with a high-index ring and a trench improves the minimum effective refractive index difference between adjacent eigenmodes and reduces the bending loss. The implementation of a double bow-tie structure enhances birefringence, resulting in a greater separation of degenerate modes. We investigated the effects of various parameters of the proposed fiber on n_{eff} between adjacent eigenmodes, min Δn_{eff}, A_{eff}, B_{m}, bending loss, and the number of supported eigenmodes at the wavelength of 1550 nm. Moreover, we evaluated n_{eff}, min Δn_{eff}, A_{eff}, DMD, and dispersion of the C+L+U band. Simulation results demonstrate that the DBT-MREC-MMF effectively splits adjacent eigenmodes by combining bow-tie stress-applying, bow-tie air holes, and multi-ring elliptical core structures. The proposed fiber achieves min Δn_{eff} between adjacent eigenmodes larger than 3.515×10^{-4} across the C+L+U band. The proposed fiber has potential applications in MIMO-free eigenmode-division multiplexing systems to increase transmission capacity and spectral efficiency. Furthermore, the proposed fiber has potential in MIMO-free eigenmode-division multiplexing systems to increase transmission capacity and spectral efficiency.

2. Fiber Design

Figure 1 presents the schematic cross-section and refractive index profile of the proposed DBT-MREC-MMF. The fiber comprises a cladding made of pure SiO_2, two bow-tie air holes, two bow-tie stress-applying areas doped with B_2O_3-doped silica, and three different step-index cores doped with GeO_2-doped silica. The refractive index difference between the elliptical core and the cladding of the fiber is denoted as Δn_1, and the long and short semi-axes of the elliptical core are a_3 and b_3, respectively. A high-index ring with the same ellipticity as the elliptical core is introduced by addition to the elliptical core. The high-index ring has an inner radius of long semi-axis a_1 and short semi-axis b_1, and an outer radius of long semi-axis a_2 and short semi-axis b_2, with a relative refractive index difference between the high-index-ring and cladding of Δn_2. Moreover, a trench layer with the same ellipticity as the core is added close to the outer side of the elliptical core, with long semi-axis a_4 and short semi-axis b_4. The relative refractive index difference between the trench and the cladding is Δn_3. The ellipticity of the core, high-index ring, and trench is defined as $e = a_1/b_1 = a_2/b_2 = a_3/b_3 = a_4/b_4$. The bow-tie stress-applying areas have parameters of an inner radius of r_1, width h, and angle θ, with an outer radius of $r_2 = r_1 + h$. The bow-tie air hole parameters have the long semi-axis a_5 and short semi-axis b_5, angle θ_0, and ellipticity $e_0 = a_5/b_5$. The refractive index of air is 1. The diameter of the fiber cladding is 125 μm.

The relative refractive index differences between the cores and cladding are denoted as $\Delta = (n_{\text{core}}^2 - n_{\text{clad}}^2)/2n_{\text{core}}^2$. The cladding material is SiO_2 with n_{eff} of 1.444 at a wavelength of 1550 nm according to the Sellmeier equation [29]. The mole fraction (mol%) of GeO_2 and

B_2O_3, corresponding to Δn_1, Δn_2, and Δn_3, and the stress-applying area refractive index can be theoretically calculated using the hybrid Sellmeier equation [29,30]. The hybrid Sellmeier equation describes the relationship between the refractive index, wavelength, and concentration of dopants.

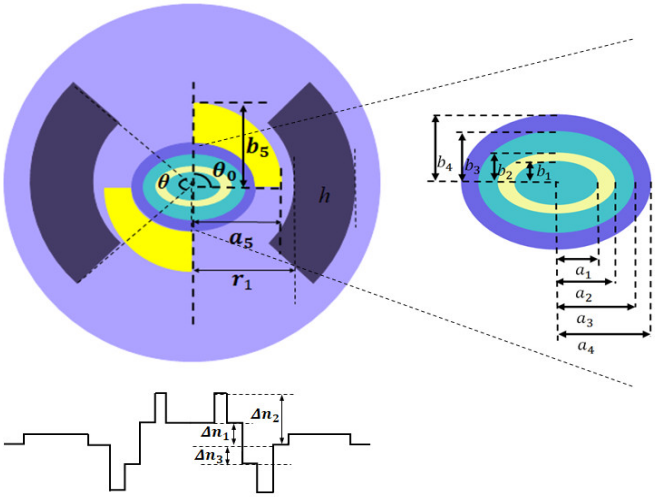

Figure 1. Schematic cross-section and refractive index profile of the DBT-MREC-MMF.

The thermal expansion coefficient (α) of the doped material is defined as $\alpha = (1 - m)\ \alpha_0 + m\alpha_1$ [31], where m and α_1 represent the mole percentage and thermal expanding coefficient of the doped material, and $1 - m$ and α_0, respectively, are the mole percentage and thermal expanding coefficient of raw material. Thermal expansion coefficients of SiO_2, GeO_2, and B_2O_3 are 5.4×10^{-7} (1/K), 7×10^{-6} (1/K), and 10×10^{-6} (1/K), respectively. In practical fiber fabrication, a 30% mol-doped fraction of B_2O_3 in the stress-applying area has been utilized [31]. Based on this calculation, the refractive index of the stress-applying area is 1.468 at 1550 nm, and the thermal expansion coefficient is 3.378×10^{-6} (1/K). Further details regarding the fiber elastic parameters are summarized in [31], including the thermal expansion coefficient (α), Young's modulus (E), Poisson's ratio (v), the first and second stress optical coefficients (C_1, C_2), and operating and reference temperature. All simulations in this work were implemented using the finite element method at a wavelength of 1550 nm.

3. Results Simulation Analysis and Optimization

The main work of this section was to optimize parameters of the proposed fiber.

3.1. Optimization of Multi-Ring Elliptical Core Parameters

Figure 2 presents the schematic cross-section of the bow-tie muti-ring elliptical multi-mode fiber (BT-MREC-MMF). In this study, we first optimized the parameters of the optical fiber without adding bow-tie air holes. That is, we optimized the parameters of the bow-tie type multi-ring elliptical core optical fiber.

We first optimized the parameters of the fiber high-index ring structure. We fixed $a_1 = 3$ μm, $a_3 = 9$ μm, $a_4 = 12$ μm, $\Delta n_1 = 0.012$, $\Delta n_2 = 0.018$, $\Delta n_3 = 0.005$, $r_1 = 20$ μm, $h = 8.9$ μm, $\theta = 90°$, and $r_2 = 28.9$ μm. The paraments a_2 and e were adjusted to optimize the Δn_{eff} between adjacent eigenmodes. The influence of a_2 and e on min Δn_{eff} and the number of supported eigenmodes are shown in Figure 3. It can be seen that the min Δn_{eff} first increases, and then decreases, with increasing a_2 and e, while the number of supported eigenmodes gradually increases with increasing a_2 and decreasing e. Within the region of 5.7 μm $\leq a_2 \leq$ 6.3 μm and $1.6 \leq e \leq 1.71$, the proposed fiber supports 22 eigenmodes, and min Δn_{eff} between adjacent eigenmodes is larger than 2.3×10^{-4}. To obtain a larger min Δn_{eff} and better-designed tolerances, we selected the middle point $a_2 = 6.1$ μm and $e = 1.65$ (i.e., $b_2 = 3.7$ μm) in the region as the parameters of the high-index ring structure,

which is marked by the red dot in Figure 3a. The preparation error ranges are ± 0.2 µm and ± 0.5 µm, respectively. The proposed MMF can support 22 eigenmodes and the effective refractive index difference between adjacent eigenmodes is greater than 2.58 × 10^{-4}.

Figure 2. Schematic cross-section of the BT-MREC-MMF.

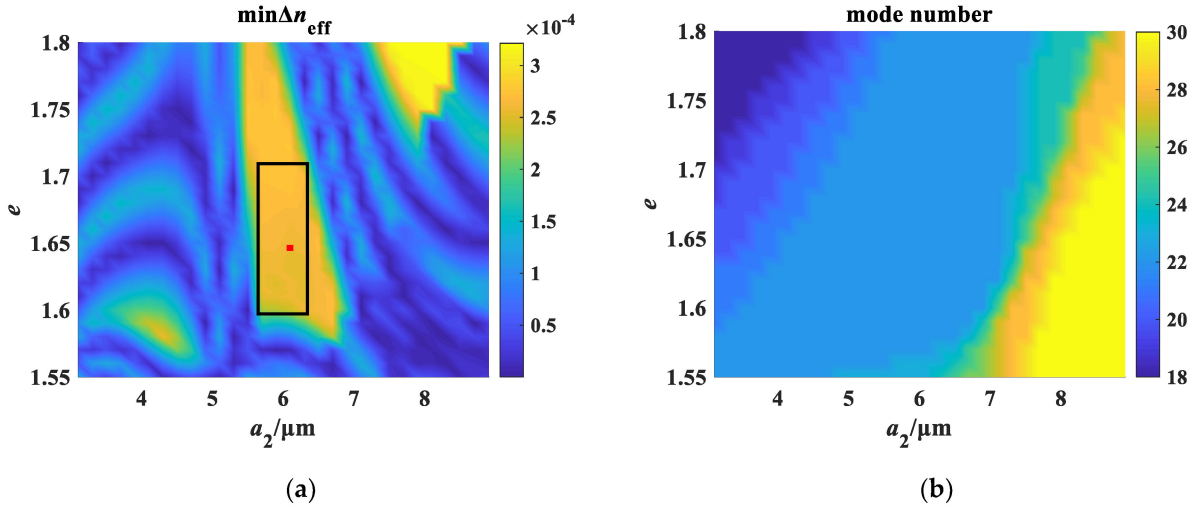

Figure 3. Variations of (**a**) the min Δn_{eff} and (**b**) mode number as a function of a_2 and e.

We continued to optimize the parameters of the high-index ring; here, we fixed a_1 = 3 µm, a_2 = 6.1 µm, a_3 = 9 µm, a_4 = 12 µm, Δn_1 = 0.012, Δn_3 = 0.005, r_1 = 20 µm, h = 8.9 µm, θ = 90°, and e = 1.65. Figure 4a,b shows variations of n_{eff} and the min Δn_{eff} as a function of the relative refractive index Δn_2 in the high-index ring. Within the range of 1.6% ≤ Δn_2 ≤ 2%, the min Δn_{eff} is related to the Δn_{eff} of the HG_{12}^{x} and HG_{12}^{y} modes. As shown in Figure 4b, with increasing Δn_2, min Δn_{eff} decreases. To obtain a larger min Δn_{eff}, we took Δn_2 = 1.8%, such that the min Δn_{eff} could reach 2.5 × 10^{-4}.

As shown in Figure 5, we investigated the influence of a_1 and a_3 on min Δn_{eff} and the number of supported eigenmodes by the fiber at a_2 = 6.1 µm, a_4 = 12 µm, Δn_1 = 0.012, Δn_3 = 0.005, r_1 = 20 µm, h = 8.9 µm, θ = 90°, and e = 1.65. From the rectangular area of Figure 5, within the region of 2.5 µm ≤ a_1 ≤ 3.6 µm and 8.4 µm ≤ a_3 ≤ 9.2 µm, the proposed fiber supports 22 eigenmodes, and the min Δn_{eff} between adjacent eigenmodes is larger than 2 × 10^{-4}. To obtain a larger min Δn_{eff} and better-designed tolerances, we chose the points a_1 = 3.3 µm (i.e., b_1 = 2 µm) and a_3 = 9 µm (i.e., b_3 = 4.45 µm) in the region as the parameters of the elliptical core. This parameter is marked by a red dot in Figure 5a. The effective refractive index difference between adjacent eigenmodes is greater than 2.58 × 10^{-4}.

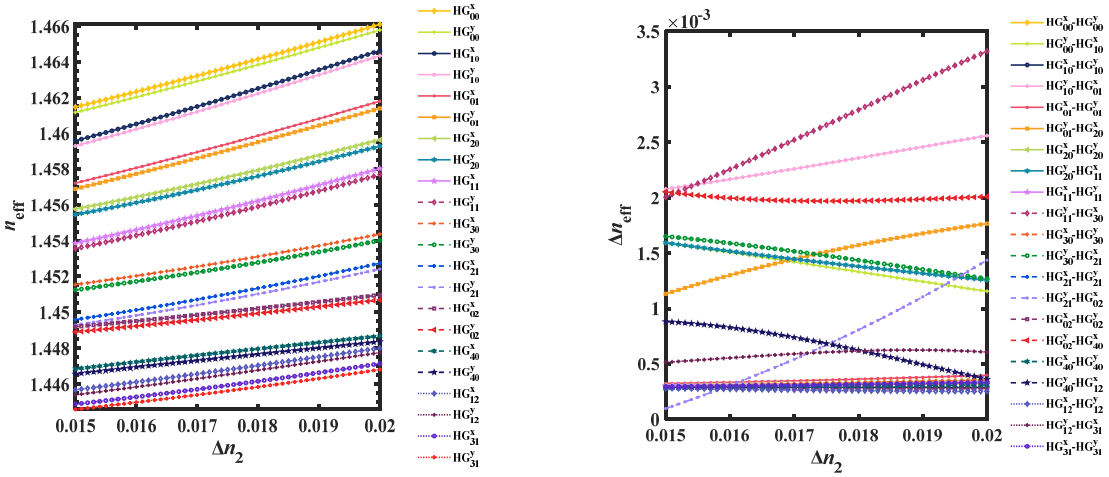

(**a**) (**b**)

Figure 4. Variations of (**a**) n_{eff} and (**b**) Δn_{eff} as a function of Δn_2.

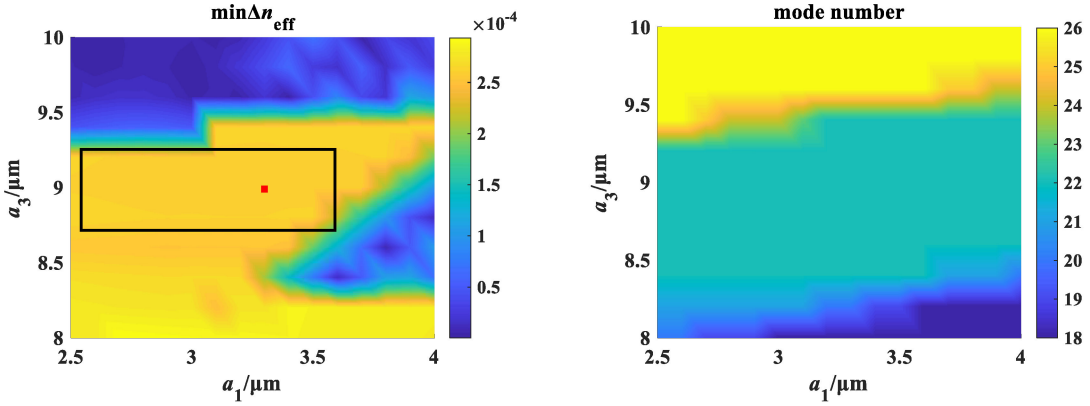

(**a**) (**b**)

Figure 5. Variations of (**a**) the min Δn_{eff} and (**b**) mode number as a function of a_1 and a_3.

We investigated the influence of the core parameter Δn_1 on Δn_{eff} at a_1 = 3.3 μm, a_2 = 6.1 μm, a_3 = 9 μm, a_4 = 12 μm, Δn_2 = 0.018, Δn_3 = 0.005, r_1 = 20 μm, h = 8.9 μm, θ = 90°, and e = 1.65, as shown in Figure 6. It can be seen that the min Δn_{eff} first increases and then decreases with increasing Δn_1. Min Δn_{eff} is larger than 2.3 × 10^{-4} within the range of 1% ≤ Δn_1 ≤ 1.48%. Here, we took Δn_1 = 1.3% to keep supporting 22 fully separated eigenmodes in the whole C+L+U band. This corresponds to a 13 % mol fraction of GeO_2 doped in SiO_2.

Adding a trench structure can effectively reduce bending loss and obtain a larger design tolerance at the same time [32]. We fixed a_1 = 3 μm, a_3 = 9 μm, a_4 = 12 μm, Δn_1 = 0.012, Δn_2 = 0.018, Δn_3 = 0.005, r_1 = 20 μm, h = 8.9 μm, θ = 90°, and e = 1.65, and adjusted a_4 and Δn_3 accordingly, to optimize min Δn_{eff} between adjacent eigenmodes. The effect of a_4 and Δn_3 on min Δn_{eff} and the number of supported eigenmodes are shown in Figure 7. Within the region of 10.25 μm ≤ a_4 ≤ 13 μm and 0.0055 ≤ Δn_3 ≤ 0.009, the proposed fiber supports 22 eigenmodes, and min Δn_{eff} between adjacent eigenmodes is larger than 2.3 × 10^{-4}. The trench has a significant effect on lifting min Δn_{eff} between adjacent eigenmodes. Considering the feasibility of the fabrication process, we chose the parameters of the red dot (a_4 = 11 μm and Δn_3 = 0.7%) for further optimization.

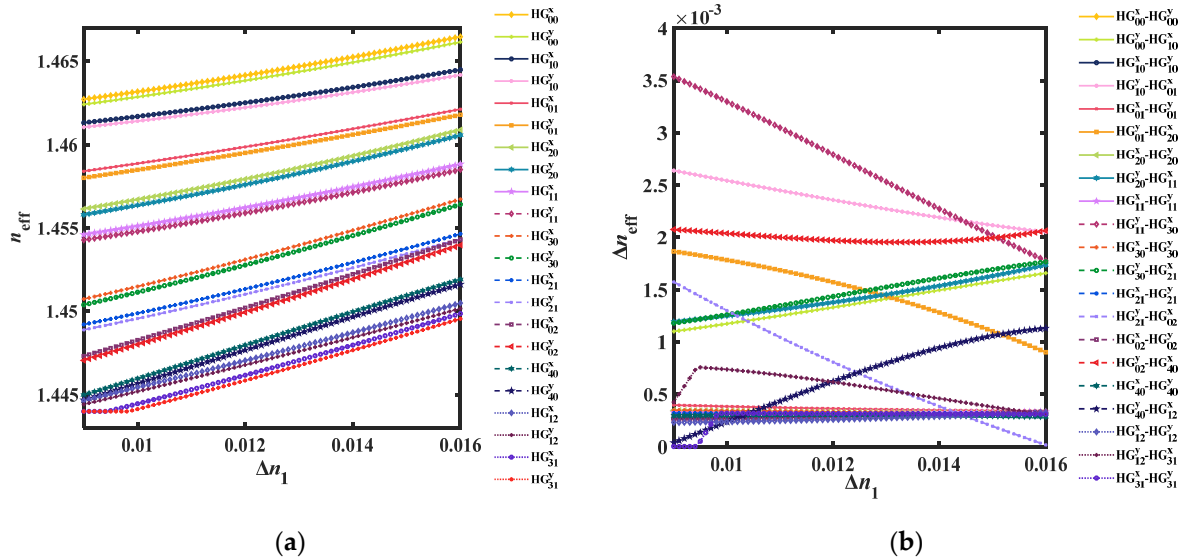

Figure 6. Variations of (**a**) n_{eff} and (**b**) Δn_{eff} as a function of Δn_1.

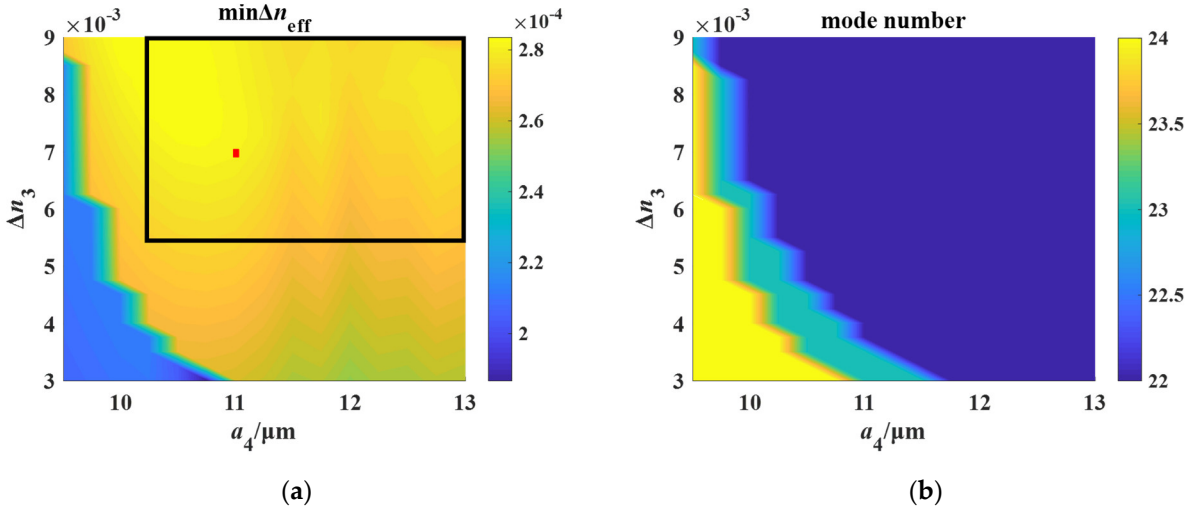

Figure 7. Variations of (**a**) the min Δn_{eff} and (**b**) mode number as a function of a_4 and Δn_4.

3.2. Optimization of Stress-Applying Parameters

To optimize the structure size of the stress-applying area, we analyzed the influence of r_1, h, and θ on Δn_{eff}, B_{m}, and bending loss. Figure 8 shows the colormaps of min Δn_{eff} versus r_1 and h with θ set as 60°, 90°, and 120°, respectively. The influence of structure parameters of optical fiber r_1, h, and θ on bending loss along the direction of the x-axis and y-axis at bending radius R = 30 mm are shown in Figure 9. It can be clearly seen that the error range gradually decreases with the increase of angle θ. B_{m} increases with increasing h and decreasing r_1. The increase in the area of the bow-tie stress-applying areas has a significant effect on improving the birefringence of the optical fiber. As shown in Figure 8b, within the region of 7 μm $\leq h \leq$ 15 μm and 16 μm $\leq r_1 \leq$ 26 μm, the proposed fiber continues to support 22 eigenmodes with a min Δn_{eff} larger than 2×10^{-4}. To obtain a larger min Δn_{eff}, lower bending loss, and larger manufacturing error range with reasonable parameter values, we finally choose the red point θ = 90°, r_1 = 20 μm, h = 11 μm as the target fiber structure size. At this point, the min Δn_{eff} value is 3.29×10^{-4}, and modal birefringence $B_{\text{m}} = 3.28 \times 10^{-4}$ N/m^2.

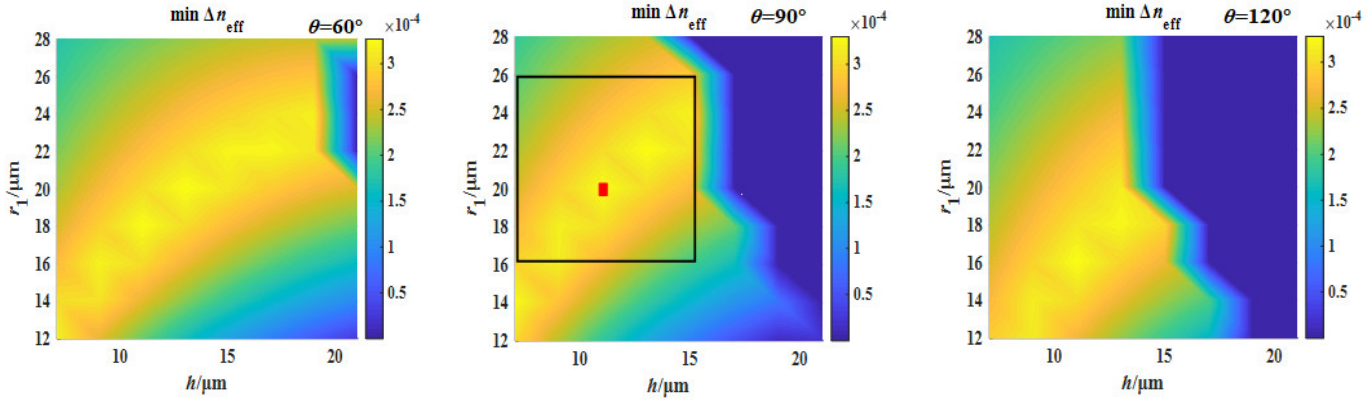

Figure 8. Min Δn_{eff} as functions of h and r_1 with θ respectively taking (**a**) 60°, (**b**) 90°, and (**c**) 120°.

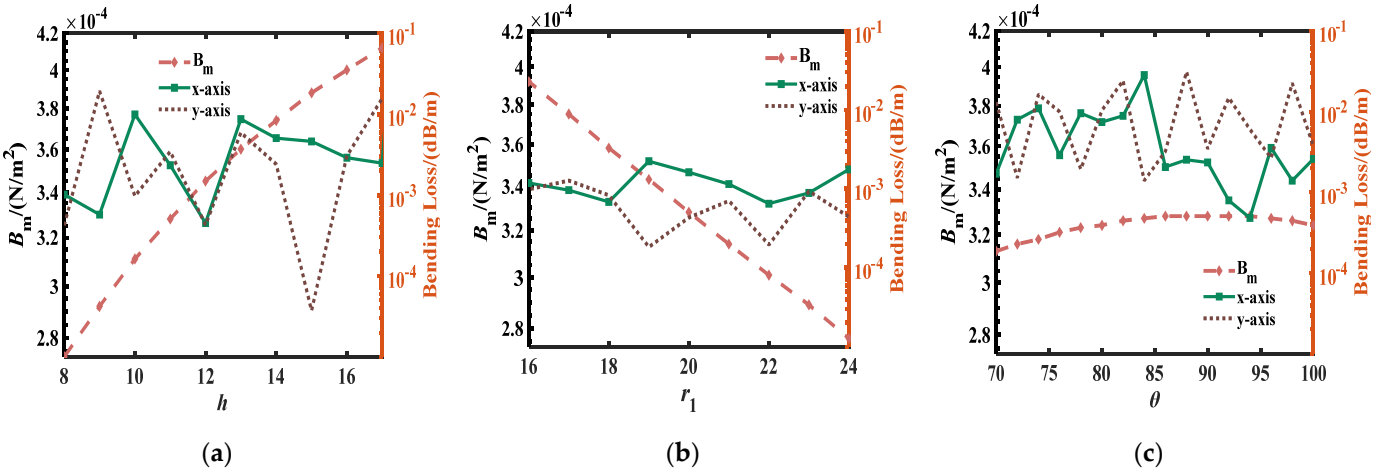

Figure 9. Variations of B_{m} (**left side**) and bending loss (**right side**) along the x-axis or y-axis direction at bending radius R = 30 mm as a function of (**a**) h, (**b**) r_1, and (**c**) θ.

3.3. Optimization of Bow-Tie Air Holes Parameters

The bow-tie air holes were introduced between the multi-ring elliptical core and the bow-tie stress-applying areas. We optimized the parameters of the bow-tie air holes of the DBT-MREC-MMF to increase min Δn_{eff} and reduce modal coupling. Figure 10 shows the colormaps of min Δn_{eff} versus e_0 and a_5, with θ_0 taking 30°, 45°, and 60°, respectively. The influence of structure parameters e_0, a_5, and θ_0 on bending loss along the direction of the x-axis and y-axis at bending radius R = 30 mm is shown in Figure 11. It can be seen from Figure 11 that B_{m} increases with the decrease of e_0 and the increase of a_5 and θ_0. This is because decreasing the ellipticity e_0 and increasing a_5 and θ_0 implies an increase in the geometric asymmetry and area of the bow-tie air hole. That leads to an increase in the contribution of geometric birefringence to overall birefringence. Considering larger min Δn_{eff}, appropriate manufacturing tolerances, and lower bending loss, e_0 = 1, a_5 = 18.5 μm, and θ_0 = 45° were selected as the parameters of the bow-tie air holes, as shown in the red dot in Figure 10b. At this point, the min Δn_{eff} value increases from 3.289 × 10^{-4} to 3.515 × 10^{-4}, and the modal birefringence value increase from 3.26 × 10^{-4} N/m^2 to 3.627 × 10^{-4} N/m^2. The results show that the introduction of bow-tie air holes effectively increases the min Δn_{eff} between adjacent eigenmodes.

In summary, we optimized the parameters of the fiber structure to support 22 eigenmodes. The results indicate that the DBT-MREC-MMF exhibits a large min Δn_{eff} between adjacent eigenmodes. We selected the optimal parameters to achieve a larger min Δn_{eff} and better-designed tolerances.

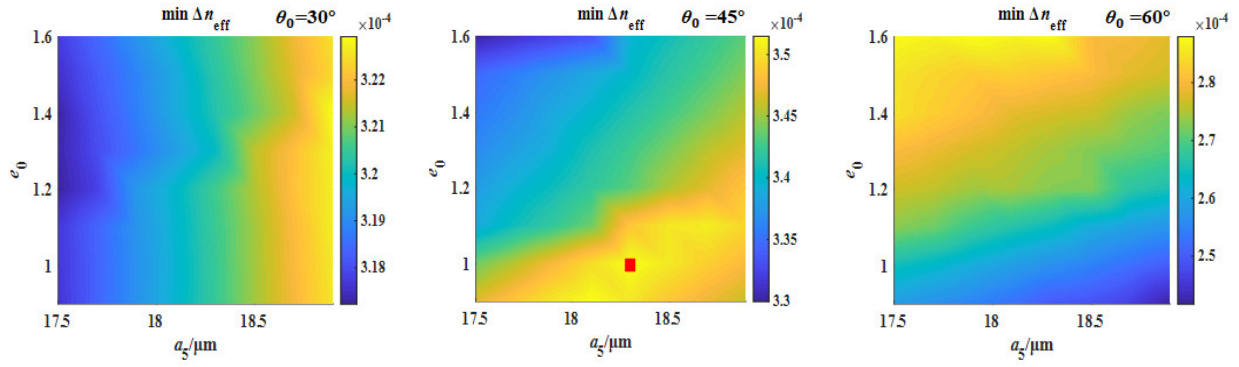

Figure 10. Min Δn_{eff} as functions of a_5 and e_0 with θ_0 respectively taking (**a**) 30°, (**b**) 45°, and (**c**) 60°.

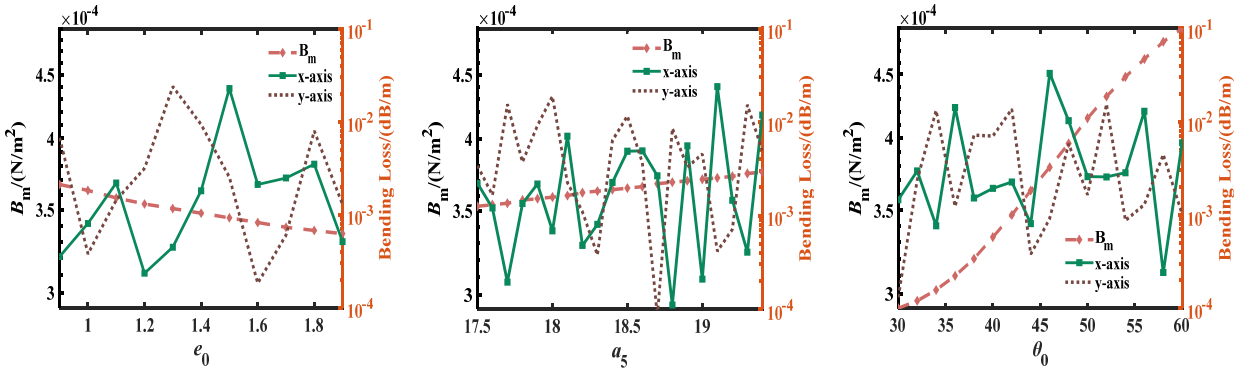

Figure 11. Variations of B_{m} (**left side**) and bending loss (**right side**) along the x-axis or y-axis direction at bending radius R = 30 mm as a function of (**a**) e_0, (**b**) a_5, and (**c**) θ_0.

4. Mode Properties and Broadband Characteristics

4.1. Birefringence

Figure 12 shows mode field intensity distributions with electric vectors (white arrows) distributions of modes supported by the DBT-MREC-MMF for all 22 eigenmodes at 1550 nm. It is apparent that all polarization directions of eigenmodes are approximately horizontal or vertical, and all the eigenmodes are well confined within the core region, which displays a superior capacity to maintain polarization.

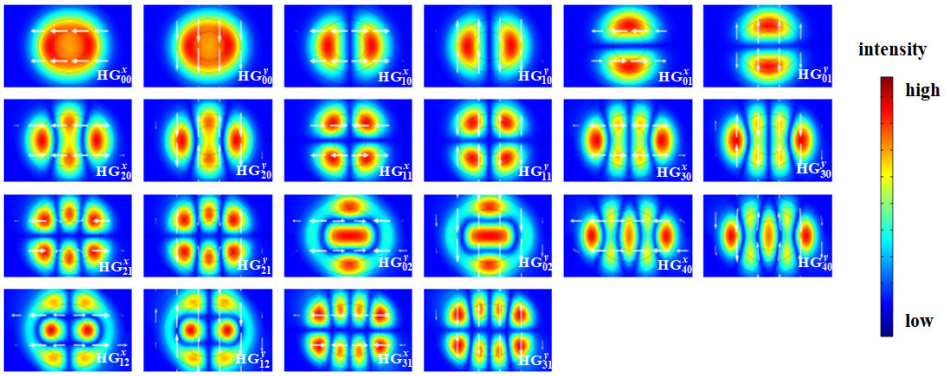

Figure 12. Model field distributions with electric vectors (white arrows) for 22 eigenmodes of the proposed DBT-MREC-MMF at the wavelength of 1550 nm.

Birefringence performance is important for studying the polarization properties of fibers. High values of birefringence provide superior polarization retention. Modal birefringence is

related to many factors, such as the size of the stress-applying area, temperature, core ellipticity, core-cladding refractive index difference, thermal expansion coefficient, and wavelength of light. When a fiber has an asymmetric structure and stress-applying areas, it is necessary to analyze its modal birefringence (B_m). B_m can be classified into two types: geometric birefringence (B_g) and stress birefringence (B_s). B_g is caused by the anisotropy of the refractive index of the material due to the asymmetry of the fiber structure. B_s is caused by the photoelastic effect in the fiber after the addition of stress-applying areas. B_m is defined as [31]:

$$B_m = N_x - N_y = B_g + B_s = N_{x0} - N_{y0} + (C_1 - C_2)(\sigma_x - \sigma_y), \quad (1)$$

where N_x and N_y are the refractive indices of the material along the x and y directions. N_{x0} and N_{y0} are the refractive indices of the stress-free material. σ_x and σ_y are the normal stress along the x and y directions of the material, respectively. C_1 and C_2 are the stress-optic coefficients. B_s is defined as:

$$B_s = (C_1 - C_2)(\sigma_1 - \sigma_2). \quad (2)$$

Figure 13a,b shows the distribution of the normal stress σ_x and σ_y in the transverse cross-section of the proposed MMF. Stress along the *x*-axis (σ_x) is much larger than that along the *y*-axis (σ_y). The normal stress along the *x*-axis (σ_x) and *y*-axis (σ_y) are ~5.38 × 10^7 N/m^2 and ~−5.19 × 10^7 N/m^2, respectively. Stress-induced birefringence, B_s = (C_1 − C_2) × (σ_x − σ_y), is ~3.626 × 10^{-4}. According to Equation (1), we obtain the B_m of each point in the cross-section of the MMF. Figure 13c,d shows the distributions of the von Mises stress distribution and geometric and stress-induced birefringence (N_x − N_y) in the transverse cross-section of the DBT-MREC-MMF. From Figure 13d, the maximum birefringence is 9.55 × 10^{-4} N/m^2, and birefringence at the core is ~3.627 × 10^{-4} N/m^2. As for the B_g, which can be derived from Equations (1) and (2), the value is ~0.001 × 10^{-4}. Since the B_s is much larger than the B_g, the main part of the B_m is B_s.

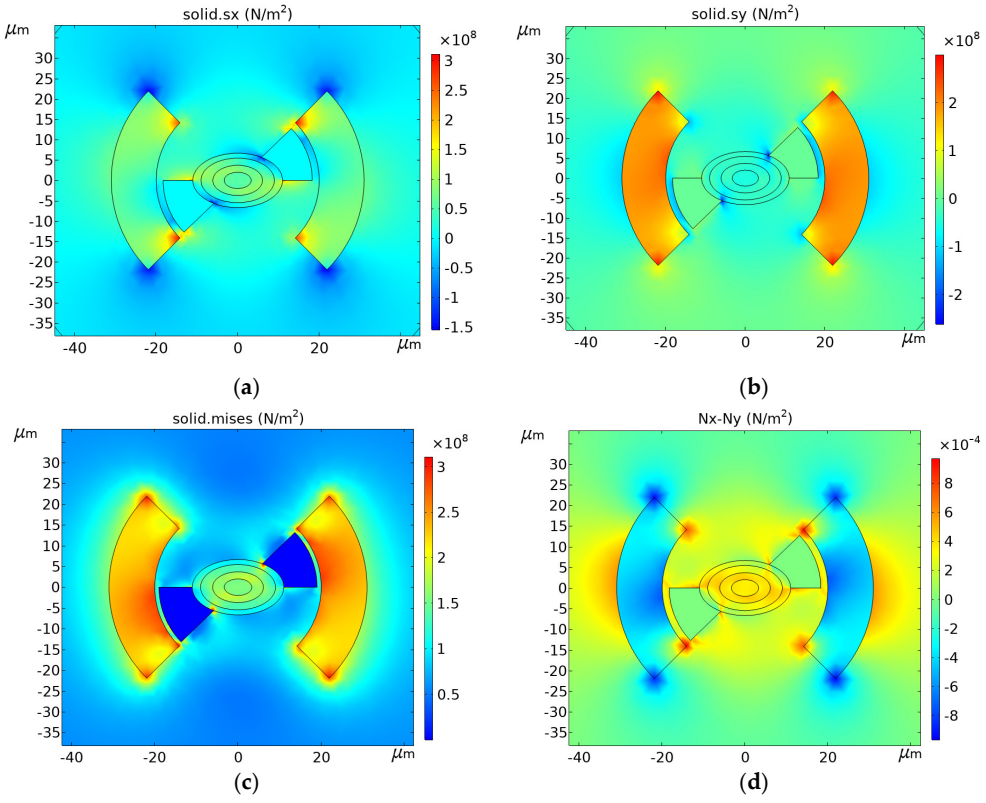

Figure 13. Distributions of (**a**) normal stress σ_x, (**b**) normal stress σ_y, (**c**) von Mises stress, and (**d**) modal birefringence Bm ($\neg_x$ − N_y) in the transverse cross-section of the proposed DBT-MREC-MMF.

4.2. Bending Loss

For fiber in the actual transmission process, the loss generated by bending will decrease the quality of signal transmission. The bending loss of each eigenmode is obtained from the imaginary part of the effective index, shown as follows [33],

$$Bending\ Loss = \frac{20 \cdot 2\pi \cdot Im(n_{\mathrm{eff}})}{ln(10) \cdot \lambda} \tag{3}$$

The DBT-MREC-MMF is asymmetric. The bending loss is different for different bending directions. The bending losses along the x and y-axis are calculated here. As shown in Figure 14, at the bending radius of 24, 22, and 10 mm along the x or y-axis, the number of eigenmodes reduces to 20, 18, and 16, respectively. Under an identical bending radius, the bending loss value of the low-order mode is lower than that of the high-order mode. When R is 30 mm, the bending loss along the x and y-axis is below 10^{-4} dB/m. Numerical results show that the proposed fiber has excellent bending resistance. When R is larger than 30 mm, the proposed fiber supports 22 eigenmodes, and the corresponding maximum bending losses of the fiber along the x and y-axis are 8.05×10^{-4} and 3.789×10^{-4} dB/m, respectively.

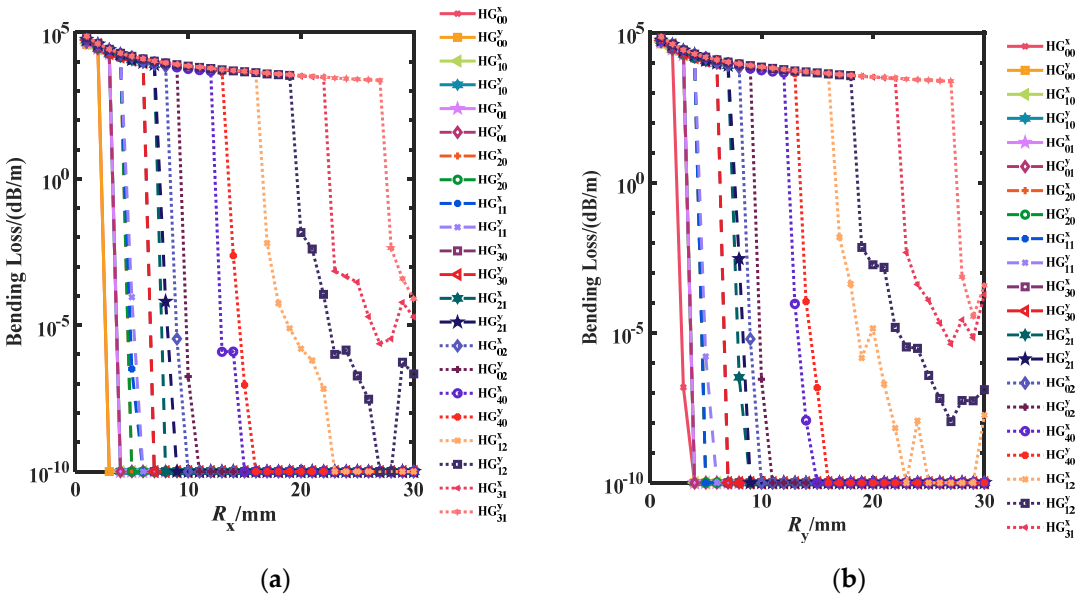

(**a**) (**b**)

Figure 14. Bending loss as a function of bending radius R along the (**a**) x-axis and (**b**) y-axis.

4.3. Broadband Performances

We further investigated the relationship between wavelength and mode properties (n_{eff}, Δn_{eff}, DMD, D, and A_{eff}) of DBT-MREC-MMF covering the whole C+L+U band. The variations of n_{eff} and Δn_{eff} as a function of the wavelength for each eigenmode are presented in Figure 15a,b. It was found that the DBT-MREC-MMF supports 22 eigenmodes over a range of wavelengths from 1530 to 1675 nm, and the min Δn_{eff} between adjacent eigenmodes is larger than 3.089×10^{-4} at 1530 nm. Results indicate that the DBT-MREC-MMF can work across the whole C+L+U band.

The differential mode delay (DMD) is important to reduce the complexity and power loss of MIMO processing. The DMD between mode A and mode B can be defined as [34]:

$$\mathrm{DMD} = \tau_{\mathrm{B}} - \tau_{\mathrm{A}} = \frac{n_{\mathrm{gB}} - n_{\mathrm{gA}}}{\mathrm{c}} = \frac{n_{\mathrm{effB}} - n_{\mathrm{effA}}}{\mathrm{c}} - \frac{\lambda}{\mathrm{c}}\left(\frac{\partial n_{\mathrm{effB}}}{\partial \lambda} - \frac{\partial n_{\mathrm{effA}}}{\partial \lambda}\right) \tag{4}$$

where τ_{B} and τ_{A} are the group time delays of the two modes, n_{gB} and n_{gA} are the group refractive indices, n_{effB} and n_{effA} are the effective refractive indices, and c and λ are the speed of light and the operating wavelength in vacuum, respectively. Fiber dispersion is a

key factor in determining transmission capacity, and the dispersion of each eigenmode is calculated by [16]:

$$D = -\frac{\lambda}{C}\frac{\partial^2 n_{eff}}{\partial \lambda^2} \quad (5)$$

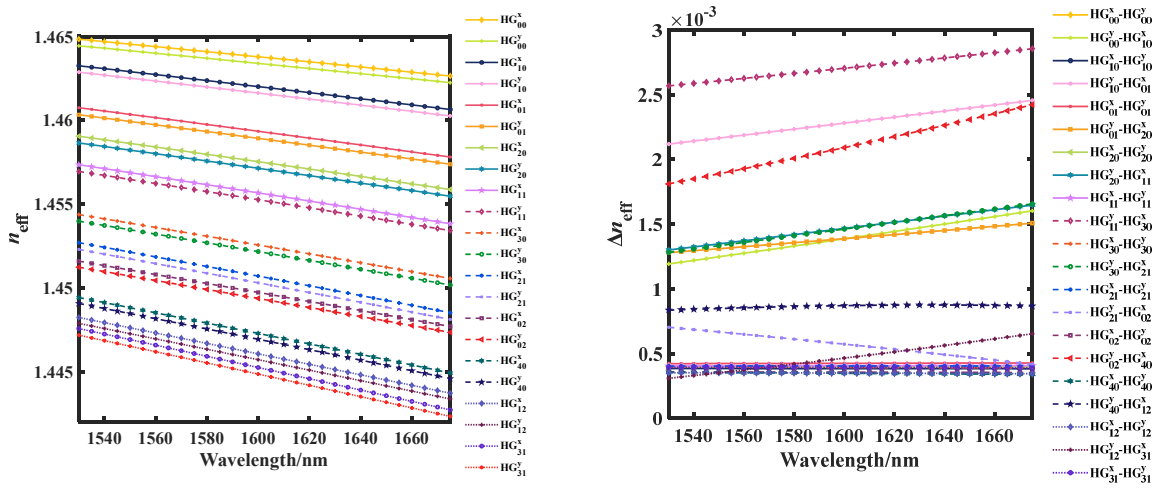

(**a**) (**b**)

Figure 15. Variations of (**a**) n_{eff} and (**b**) min Δn_{eff} as a function of wavelength.

As shown in Figure 16a,b, the DMD and dispersion of all 22 eigenmodes as a function of wavelength were calculated. All of the eigenmodes exhibit a relatively small DMD (−15.41~12.4 ns/km), which can induce negligible power penalties in short-haul optical communication links. Moreover, the dispersion values for lower-order eigenmodes covering the whole C+L+U band vary from 17.39 to 63.75 ps/nm/km, indicating that dispersion can be neglected when applied in short-haul optical interconnects. The dispersion value for higher-order eigenmode HG_{31}^{y} is larger, and ranges from −77.57 to −70.85 ps/nm/km over the whole C+L+U band. To compensate for the dispersion problem in fibers, specialized dispersion-compensating fibers can be used. This method helps to ensure that the signal transmitted through the fibers remains intact and undistorted, enabling high-quality data transmission [35–37]. Hence, this fiber can be considered to be a promising candidate for MIMO-free MDM systems.

The mode effective area (A_{eff}) of the fiber reflects the lateral distribution of the optical field on the fiber cross-section. The nonlinear coefficient and A_{eff} are reciprocal to each other. A_{eff} is calculated by Equation (6) [38]:

$$A_{eff} = \frac{\left(\iint |E|^2 dxdy\right)^2}{\iint |E|^4 dxdy} \quad (6)$$

where E represents the mode field power distribution across the fiber cross-section wavelength. The A_{eff} of the proposed DRT-MREC-MMF within the wavelength range of 1530 to 1675 nm is shown in Figure 17. The effective area gradually increases with increasing wavelength. The A_{eff} values range from 66.8 to 96.39 μm^2 over the whole C+L+U band.

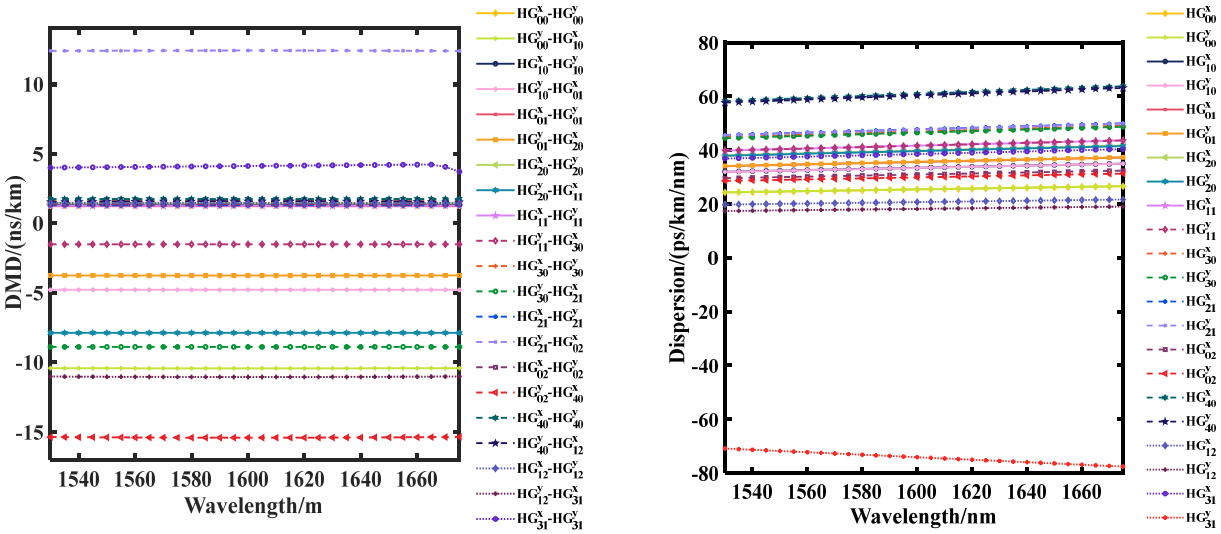

Figure 16. Variations of (**a**) DMD and (**b**) dispersion as a function of wavelength.

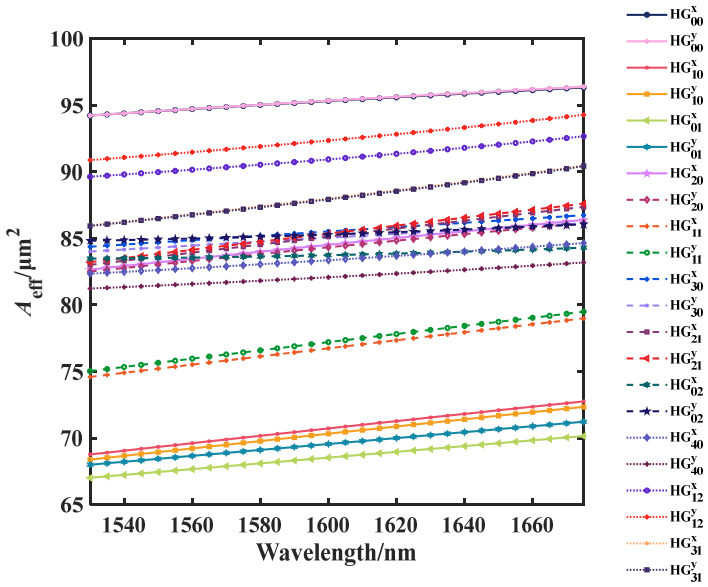

Figure 17. Variations of A_{eff} as a function of wavelength.

5. Fabrication Method and Tolerance

Table 1 clearly lists the tolerance parameters of the DBT-MREC-MMF. The min Δn_{eff} of the target value is 3.515×10^{-4}. It is noteworthy that, within all the tolerance ranges listed in Table 1, the value of min Δn_{eff} is greater than 2×10^{-4}, and the fiber supports 22 eigenmodes. These results demonstrate that the fiber exhibits a considerably high tolerance and exceptional performance.

Table 1. Optimal parameters with fabrication tolerance of the DBT-MREC-MMF.

	Tolerance Range	Target Value		Tolerance Range	Target Value		Tolerance Range	Target Value
$a_2/\mu m$	5.7~6.3	6.1	e	1.6~1.71	1.65	Δn_2	0.016~0.02	1.78
$a_1/\mu m$	2.5~3.6	3.3	$a_3/\mu m$	8.4~9.2	9	Δn_1	0.01~0.0148	0.013
$a_4/\mu m$	10.25~13	11	Δn_3	0.0055~0.009	0.007	$h/\mu m$	7–15	11
$r_1/\mu m$	16~26	20	θ	70~100	90	e_0	0.9~1.9	1
$a_5/\mu m$	17.5~20.5	18.5	θ_0	30~60	45			

The fabrication process of the proposed weakly-coupled DBT-MREC-MMF typically involves the following steps: (1) Preform fabrication: The first step is to fabricate a preform of the proposed fiber structure. This is typically done using the modified chemical vapor deposition (MCVD) method, where a glass tube is heated and rotated while reactive gases are introduced to deposit the desired dopants and form the core and cladding. (2) Drawing the fiber: After the preform is fabricated, it is placed in a fiber drawing tower where it is heated and drawn into a thin fiber. The fiber diameter is controlled by the drawing speed and the temperature gradient along the preform. (3) Etching: Once the fiber is drawn, it is etched to create the air-hole structure. This can be done using hydrofluoric acid or a similar etchant, which selectively removes the cladding material around the air holes. (4) Cleaving and polishing: The final step is to cleave the fiber to the desired length and polish the end faces to ensure good optical coupling.

Several novel ring core fibers have been successfully developed [39,40], exhibiting excellent performance in data transmission. The fabrication process of stress-applying regions, particularly the widely experimented bow-tie or panda-type in polarization-maintaining fibers, has reached a mature stage [41,42]. Additionally, air-hole-assisted fibers have been extensively studied and manufactured [43,44]. Drawing on these well-established fabrication techniques and experiences, it is reasonable to suggest that the proposed fully degeneracy-lifted DBT-MREC-MMF for MIMO-free direct fiber MDM transmission could be manufactured. We are confident that the fabrication of the proposed fiber will be successfully realized.

6. Conclusions

In conclusion, we have presented a weakly-coupled double bow-tie multi-ring elliptical core multi-mode fiber capable of supporting 22 independent eigenmodes across the C+L+U band. The proposed fiber structure, incorporating bow-tie air holes, a multi-ring elliptical core, and bow-tie stress-applying areas, exhibits enhanced modal birefringence and effectively separates adjacent eigenmodes. The proposed fiber design utilizes a multi-ring elliptical core created by inserting a high-index ring and adding an outer trench, resulting in improved separation and transmission between adjacent eigenmodes. The bow-tie air holes lead to enhanced modal birefringence and improved separation of adjacent eigenmodes. The bow-tie stress-applying areas induce stress on the fiber, further enhancing modal birefringence and improving polarization maintaining performance.

Through parameter optimization, the proposed fiber achieves a Δn_{eff} between adjacent eigenmodes larger than 3.089×10^{-4} over the whole C+L+U band. The fiber has a high effective area (66.8~96.39 μm^2), low differential mode delay (-15.41~12.4 ns/km), and negligible bending loss ($<10^{-4}$ dB/m). Overall, our simulation results suggest that the proposed DBT-MREC-MMF holds great promise for applications in eigenmode-division multiplexing transmission, offering significant bandwidth improvements and increased transmission capacity. By analyzing and optimizing the structural parameters, the proposed fiber has potential applications in eigenmode-division multiplexing transmission to increase bandwidth and improve transmission capacity.

Author Contributions: Conceptualization, F.R. and Y.C.; methodology, F.R.; software, Y.C.; validation, X.L.; investigation, Y.C.; data curation, Y.L. and D.Z.; writing—original draft preparation, Y.C.; writing—review and editing, X.L.; supervision, J.W. All authors have read and agreed to the published version of the manuscript.

Funding: This research was funded by the Fundamental Research Funds for the Central Universities (FRF-TP-19-016A2).

Institutional Review Board Statement: Not applicable.

Informed Consent Statement: Not applicable.

Data Availability Statement: The data presented in this study are available upon reasonable request.

Conflicts of Interest: The authors declare no conflict of interest.

References

1. Zhong, K.; Zhou, X.; Huo, J.; Yu, C.; Lu, C.; Lau, A.P.T. Digital Signal Processing for Short-Reach Optical Communications: A Review of Current Technologies and Future Trends. *J. Light. Technol.* **2018**, *36*, 377–400. [CrossRef]
2. Gao, Y.; Li, Y.; Li, X.; Zheng, H.; Bai, C.; Hu, W.; Xu, H.; Dong, Q.; Xing, H.; Su, Y.; et al. An Elliptical-Core Few-Mode Fiber with Low Loss and Low Crosstalk for the MIMO-FREE Applications. *Front. Phys.* **2022**, *9*, 845. [CrossRef]
3. Schares, L.; Lee, B.G.; Checconi, F.; Budd, R.; Rylyakov, A.; Dupuis, N.; Petrini, F.; Schow, C.L.; Fuentes, P.; Mattes, O.; et al. A Throughput-Optimized Optical Network for Data-Intensive Computing. *IEEE Micro* **2014**, *34*, 52–63. [CrossRef]
4. Huang, M.-F.; Tanaka, A.; Ip, E.; Huang, Y.-K.; Qian, D.; Zhang, Y.; Zhang, S.; Ji, P.N.; Djordjevic, I.B.; Wang, T.; et al. Terabit/s Nyquist Superchannels in High Capacity Fiber Field Trials Using DP-16QAM and DP-8QAM Modulation Formats. *J. Light. Technol.* **2014**, *32*, 776–782. [CrossRef]
5. Essiambre, R.-J.; Kramer, G.; Winzer, P.J.; Foschini, G.J.; Goebel, B. Capacity Limits of Optical Fiber Networks. *J. Light. Technol.* **2010**, *28*, 662–701. [CrossRef]
6. Richardson, D.J.; Fini, J.M.; Nelson, L.E. Space-division multiplexing in optical fibres. *Nat. Photonics* **2013**, *7*, 354–362. [CrossRef]
7. Yu, S. Potentials and challenges of using orbital angular momentum communications in optical interconnects. *Opt. Express* **2015**, *23*, 3075–3087. [CrossRef]
8. Yang, Y.; Gao, J.; Fu, S.; Zhang, X.; Tang, M.; Tong, W.; Liu, D. PANDA Type Four-Core Fiber with the Efficient Use of Stress Rods. *IEEE Photonics J.* **2019**, *11*, 1–9. [CrossRef]
9. Corsi, A.; Chang, J.H.; Wang, R.H.; Wang, L.X.; Rusch, L.A.; LaRochelle, S. Highly elliptical core fiber with stress-induced birefringence for mode multiplexing. *Opt. Lett.* **2020**, *45*, 2822–2825. [CrossRef]
10. Wang, L.; Nejad, R.M.; Corsi, A.; Lin, J.; Messaddeq, Y.; Rusch, L.A.; LaRochelle, S. MIMO-Free transmission over six vector modes in a polarization maintaining elliptical ring core fiber. In Proceedings of the Optical Fiber Communication Conference and Exhibition, Los Angeles, CA, USA, 19–23 March 2017.
11. Xia, C.; Bai, N.; Ozdur, I.; Zhou, X.; Li, G.F. Supermodes for optical transmission. *Opt. Express* **2011**, *19*, 16653–16664. [CrossRef]
12. Arik, S.O.; Kahn, J.M.; Ho, K.-P. MIMO Signal Processing for Mode-Division Multiplexing: An Overview of Channel Models and Signal Processing Architectures. *IEEE Signal Process. Mag.* **2014**, *31*, 25–34. [CrossRef]
13. Wang, L.; Nejad, R.M.; Corsi, A.; Lin, J.; Larochelle, S. Linearly polarized vector modes: Enabling mimo-free mode-division multiplexing. *Opt. Exp.* **2017**, *25*, 11736–11749. [CrossRef]
14. Chen, S.; Tong, Y.; Tian, H.P. Eight-mode ring-core few-mode fiber using cross-arranged different-material-filling side holes. *Appl. Opt.* **2020**, *59*, 4634–4641.
15. Corsi, A.; Chang, J.H.; Rusch, L.A.; LaRochelle, S. Design of a ten-mode polarization-maintaining few-mode fiber for MIMO-less data transmission. In Proceedings of the European Conference on Optical Communication, Rome, Italy, 23–27 September 2018.
16. Zhang, X.Q.; Jiang, Y.; Xu, Y.; Chen, R.S.; Wang, A.T.; Ming, H.; Zhao, W.S. Polarization-maintaining fiber composed of an elliptical ring core and two circular air holes. *Appl. Opt.* **2019**, *58*, 8865–8870. [CrossRef]
17. Zhao, J.; Tang, M.; Kyunghwan, O.H.; Feng, Z.; Zhao, C.; Liao, R.; Fu, S.; Shum, P.; Liu, D. Polarization-maintaining few mode fiber composed of a central circular-hole and an elliptical-ring core. *Photonics Res.* **2017**, *5*, 261–266. [CrossRef]
18. Vigneswaran, D.; Mani Rajan, M.S.; Ayyanar, N.; Patel, S.K. Numerical investigation of dual guided elliptical ring core few-mode fiber for space division multiplexing applications. *Optik* **2021**, *228*, 166111. [CrossRef]
19. Yan, H.; Li, S.; Xie, Z.; Zheng, X.; Zhang, H.; Zhou, B. Design of PANDA ring-core fiber with 10 polarization-maintaining modes. *Photonics Res.* **2016**, *5*, 1–5. [CrossRef]
20. Zhang, J.; Ren, F.; Niu, J.; Lei, X.; Zhang, Y.; Cui, F.; Wang, J. Design of weakly coupled 20-eigenmode bow-tie rectangular dual-step fiber for short-haul communication in O band. *Opt. Eng.* **2021**, *60*, 126107. [CrossRef]
21. Li, H.S.; Xiao, H.; Ren, G.B. Polarization-maintaining few-mode optical fibers with air-hole structures. In Proceedings of the Asia Commun Photon, Hangzhou, China, 26–29 October 2018.
22. Li, H.; Wang, C.; An, H. Numerical simulation of the heavily Ge-doped polarization-maintaining fiber with normal dispersion. *Optoelectron. Lett.* **2022**, *18*, 35–42. [CrossRef]
23. Wang, C.; Li, H.; Qiao, Y.; An, H.; Bache, M. Normal-dispersion CS2-filled silica fiber with broadband single-polarization property. *Opt. Fiber Technol.* **2021**, *66*, 102665. [CrossRef]
24. Zhang, J.; Chen, Y.K.; Wu, Z.C.; Feng, S.J.; Shum, P.; Huang, T.Y. Panda type separated-circles-formed elliptical ring core few-mode fiber. *Opt. Fiber Technol.* **2022**, *73*, 103067. [CrossRef]
25. Du, Z.Y.; Wang, C.C.; Li, P.X.; Li, P.; Zheng, J.J.; Ning, T.G. Fully degeneracy-lifted PANDA few-mode fiber based on the segmented ring-core. *Optik* **2022**, *255*, 168710. [CrossRef]
26. Yang, T.X.; Zhang, H.; Xi, L.X.; Yang, J.X.; Chen, Z.; Wang, X.Q.; Zhang, X.G. Design of a novel bow-tie polarization ring-core few-mode fiber for MIMO-free MDM system. In Proceedings of the 26th Optoelectronics and Communications Conference, Hong Kong, China, 3–7 July 2021.
27. Behera, B.; Varshney, S.K.; Mohanty, M.N. Design of ultra-dispersion flattened M-type few-mode fiber for weakly-coupled mode division multiplexing transmission. *Optik* **2022**, *260*, 169040. [CrossRef]
28. Han, J.; Zhang, J. Design of cladding rods-assisted depressed-core few-mode fibers with improved modal spacing. *Opt. Fiber Technol.* **2018**, *41*, 131–138. [CrossRef]
29. Fleming, J.W. Dispersion in GeO_2-SiO_2 glasses. *Appl. Opt.* **1984**, *24*, 4486–4493. [CrossRef]

30. Wemple, S.H.; Pinnow, D.A.; Rich, T.C.; Jaeger, R.E.; Van Uitert, L.G. Binary SiO_2–B_2O_3 glass system: Refractive index behavior and energy gap considerations. *J. Appl. Phys.* **1973**, *44*, 5432–5437. [CrossRef]
31. Guan, R.; Zhu, F.; Gan, Z.; Huang, D.; Liu, S. Stress birefringence analysis of polarization maintaining optical fibers. *Opt. Fiber Technol.* **2005**, *11*, 240–254. [CrossRef]
32. Molin, D.; Bigot-Astruc, M.; de Jongh, K.; Sillard, P. Trench-assisted bend-resistant OM4 multi-mode fibers. In Proceedings of the 36th European Conference and Exhibition on Optical Communication, Turin, Italy, 19–23 September 2010.
33. Saitoh, K.; Koshiba, M. Leakage loss and group velocity dispersion in air-core photonic bandgap fibers. *Opt. Express* **2003**, *11*, 3100–3109. [CrossRef]
34. Kasahara, M.; Saitoh, K.; Sakamoto, T.; Hanzawa, N.; Matsui, T.; Tsujikawa, K.; Yamamoto, F. Design of Three-Spatial-Mode Ring-Core Fiber. *J. Light. Technol.* **2014**, *32*, 1337–1343. [CrossRef]
35. Doran, N.J.; Sugden, K.; Bennion, I.; Williams, J.A.R. Fibre dispersion compensation using a chirped in-fibre Bragg grating. *Electron. Lett.* **1994**, *3420*, 985–987.
36. Li, R.D.; Kumar, P.; Kath, W.L. Dispersion compensation with phase-sensitive optical amplifiers. *J. Light. Technol.* **1994**, *12*, 541–549.
37. Noe, R.; Sandel, D.; Yoshida-Dierolf, M.; Hinz, S.; Mirvoda, V.; Schopflin, A.; Gungener, C.; Gottwald, E.; Scheerer, C.; Fischer, G. Polarization mode dispersion compensation at 10, 20, and 40 gb/s with various optical equalizers. *J. Light. Technol.* **1999**, *17*, 1602–1616. [CrossRef]
38. Wang, X.; Lou, S.; Lu, W.; Sheng, X.; Zhao, T.; Hua, P. Bend Resistant Large Mode Area Fiber with Multi-Trench in the Core. *IEEE J. Sel. Top. Quantum Electron.* **2016**, *22*, 117–124. [CrossRef]
39. Brunet, C.; Vaity, P.; Ung, B.; Messaddeq, Y.; LaRochelle, S.; Rusch, L.A. Design of a family of ring-core fiber for OAM. In Proceedings of the Optical Fiber Communications Conference and Exhibition, Los Angeles, CA, USA, 22–26 March 2015.
40. Jung, Y.; Kang, Q.; Zhou, H.; Rui, Z.; Su, C.; Wang, H.; Yang, Y.; Jin, X.; Payne, F.P.; Alam, S.; et al. Low-loss 25.3 km few-mode ring-core fibre for mode-division multiplexed transmission. *J. Light. Technol.* **2017**, *35*, 1363–1368. [CrossRef]
41. Yu, Q.R.; Bao, X.Y.; Chen, L. Temperature dependence of Brillouin frequency, power, and bandwidth in panda, bow-tie, and tiger polarization-maintaining fibers. *Opt. Let.* **2004**, *29*, 17–19. [CrossRef]
42. Zhang, K.; Chang, D.Y.; Fu, Y.J.; Wei, H.; Wei, Y.; Yan, F.P.; Lou, S.Q.; Ning, T.G.; Jian, W.; Jian, S.S. Design and fabrication of Panda-type erbium-doped polarization-maintaining fibres. *Chin. Phys.* **2007**, *16*, 478–484.
43. Ziolowicz, A.; Szymanski, M.; Ostrowski, L.; Napierala, M.; Poturaj, K.; Makara, M.; Mergo, P.; Nasilowski, T. Bend insensitive hole-assisted multicore fibre for next generation transmission systems. In Proceedings of the European Conference on Lasers and Electro-Optics-European Quantum Electronics Conference, Munich, Germany, 21–25 June 2015.
44. Ma, L.; Tsujikawa, K.; Hanzawa, N.; Aozasa, S.; Nozoe, S.; Yamamoto, F. Design and Fabrication of Low Loss Hole-Assisted Few-Mode Fibers with Consideration of Surface Imperfection of Air Holes. *J. Light. Technol.* **2016**, *34*, 5164–5169. [CrossRef]